Appl Nanosci
DOI 10.1007/s13204-017-0601-z

ORIGINAL ARTICLE

Applicable anode based on Co_3O_4–$SrCO_3$ heterostructure nanorods-incorporated CNFs with low-onset potential for DUFCs

Zafar Khan Ghouri[1] · Khaled Elsaid[2] · Saeed Al-Meer[1] · Nasser A. M. Barakat[3,4]

Received: 30 July 2017 / Accepted: 14 September 2017

Abstract Besides the high-current density, lower onset potential of urea electrooxidation is key parameter which influences the direct urea fuel cell performance. In the present article, low-onset potential has been reported for nickel-free (NF) electrocatalyst in urea electrooxidation. The nickel-free electrocatalyst: Co_3O_4–$SrCO_3$ heterostructure nanorods-incorporated carbon nanofibers (CNFs) were synthesized by electrospinning technique, followed by calcination of electrospun mat composed of strontium acetate, cobalt acetate, and poly(vinyl alcohol) sol–gel in inert environment at 750 °C. Physiochemical characterizations confirmed the formation of Co_3O_4–$SrCO_3$ heterostructure nanorods-incorporated CNFs. The electrochemical activity of resultant nickel-free electrocatalyst toward the electrooxidation of urea in alkaline medium is evaluated using cyclic voltammetry measurements (CV). Co_3O_4–$SrCO_3$ heterostructure nanorods-incorporated CNFs reveals high-current density of 21.33 mA/cm^2 at low-fuel concentration. Notably, the low-onset potential has been observed, showing a good application prospect in direct urea fuel cells.

Keywords Electrospinning · Urea · DUFC · Onset potential · Electrocatalyst · Current density

Introduction

The ultimate rising requirement for energy and environmental concerns has driven the search for new resources to produce eco-friendly energy (Ghouri et al. 2015). Foregoing research demonstrated that direct liquid fuel cells (DLFCs) are a competitive alternative resource of green energy (Radenahmad et al. 2016). Among all types of direct liquid fuel cells, direct urea fuel cell (DUFCs) is a strong candidate working simultaneously for resolving energy and environmental problems (Xu et al. 2016). Besides urea fuel cell, other liquid fuel cells, such as methanol, ethanol, and formic acid fuel cells, need a supply of fuels from process industry by chemical or biological production, which requires strong storage and transportation infrastructure. For instance, direct urea fuel cells have many advantages compared to the above-mentioned liquid fuel cells, such as urea, which are not expensive, available in solid granules and, thus, easy to transport and store (Lan and Tao 2011). More interestingly, urea contains 10 wt% hydrogen with high-energy density (16.9 MJ l^{-1}) (Lan and Tao 2011; Xu et al. 2014; Lan et al. 2010). Moreover, urea is the main nitrogen-containing component in the urine/liquid waste (2–2.5 wt%) (Lan et al. 2010; Kojima et al. 2006; Boggs et al. 2009). The total theoretical cell potential of urea oxidation (0.37 V vs SHE) is much lower

✉ Zafar Khan Ghouri
zafarkhan.ghouri@qu.edu.qa;
zafarkhanghouri@hotmail.com

✉ Saeed Al-Meer
salmeer@qu.edu.qa

✉ Nasser A. M. Barakat
nasser@jbnu.ac.kr

[1] Central Laboratories Unit, Qatar University, PO Box 2713, Doha, Qatar

[2] Chemical Engineering Program, Texas A&M University at Qatar, PO 23874, Doha, Qatar

[3] Department of Organic Materials and Fiber Engineering, Chonbuk National University, Jeonju 54896, Republic of Korea

[4] Department of Chemical Engineering, Minia University, El-Minia, Egypt

Published online: 25 September 2017

than that of water electrolysis (1.23 V vs SHE), providing a cheaper source of hydrogen production (Boggs et al. 2009; King and Botte 2011). Therefore, it has been reported that either hydrogen or electricity can be generated from urea-rich aqueous solution, according to following reactions (King and Botte 2011; Wang et al. 2013).

$$\text{Anode}: \ CO(NH_2)_2 + 6OH^- \rightarrow N_2 + 5H_2O + CO_2 + 6e \quad E^0 = -0.746 \text{ V} \tag{1}$$

$$\text{Cathode}: \ 2H_2O + O_2 + 4e \rightarrow 4OH^- \quad E^0 = +0.40 \text{ V} \tag{2}$$

$$\text{Overall}: \ 2CO(NH_2)_2 + 3O_2 \rightarrow 2N_2 + 4H_2O + 2CO_2 \quad E^0 = +1.146 \text{ V} \tag{3}$$

Unfortunately, the use of costly noble metals as an anode material not only limits their possible application for urea oxidation in industrial-scale, but also exhibited low-current densities with high over potentials (Boggs et al. 2009).Among various non-precious metals, nickel-based catalyst was found to be very successful, but the transformation of E^{2+}_{Ni}/E^{3+}_{Ni} proceeds at a high potential that will directly affect the current density and energy efficiency of urea fuel cells (Xu et al. 2016; Chen et al. 2015; Guo et al. 2015). Hence, it is desirable to synthesize nickel-free (NF) catalysts that can oxidize urea efficiently at lower over potential. Recently, co-based electrocatalysts have been studied significantly. In particular, tricobalt tetraoxide (Co_3O_4), a magnetic p-type semiconductor, is a versatile inorganic transition metal oxide that has received extensive attention recently for the potential applications in many fields, including fuel cells, supercapacitors, lithium ion batteries, photocatalysis, and electrochemical sensors (Hu et al. 2008; Shahid et al. 2014; Jiao and Frei 2009; Li et al. 2005, 2008; Kim et al. 2014). In addition, co-based nanostructures as electrocatalysts supported on carbon nanofibers have appealed great attention due to its distinct characteristics over the other structures (Ghouri et al. 2015; Ghouri et al. 2016). Inspired by cobalt's catalytic activity toward electrode reactions and potential applications of $SrCO_3$ in material chemistry, we propose to develop a bimetallic catalyst, composed of cobalt oxide (Co_3O_4) and strontium carbonate ($SrCO_3$), which could potentially oxidize urea efficiently at lower onset potential and thus support to improve the overall efficiency of direct urea-based fuel cells. In this context, we develop a simple strategy to fabricate Co_3O_4–$SrCO_3$ heterostructure nanorods supported by carbon nanofibers (CNFs) as efficient nickel-free electrocatalysts via electrospinning.

Experimental

Catalyst synthesis, characterizations, and electrochemical measurements

In a typical synthesis, 0.3 g of strontium acetate (99.9%) and 0.7 g of cobalt(II) acetate tetrahydrate (98%) salts were dissolved in 3 mL of deionized water, 15 g of PVA (10 wt%) solution was added and stirred at 50 °C for 6 h, and the resultant solution was electrospun at 22 kV. Finally, after conventional drying, nanofiber mat was annealed at 750 °C for 6 h in inert environment.

The detailed physiochemical characterizations were done by field-emission scanning electron microscopy (FESEM), Raman spectroscopy, Fourier transform infrared spectroscopy (FTIR), X-ray diffraction (XRD), and thermal gravimetric analysis (TGA) measurements. Electrochemical measurements were carried out using 2 mg of active material on an electrochemical workstation (VersaSTAT 4, USA) with a three-electrode cell at room temperature.

Results and discussion

The XRD pattern of synthesized Co_3O_4–$SrCO_3$ heterostructure nanorods-incorporated CNFs are shown in Fig. 1. The apparent diffraction peaks observed at 2θ values of 25.20°, 35.02°, 44.10°, 47.83°, and 50.37 indexing as the (111), (200), (221), (212), and (231) reflection planes, respectively, conformed the formation of pure orthorhombic strontianite (JCPDS no.: 84-0418). The additional diffraction peaks at 2θ values of 31.40°, 36.90°, 44.70°, 55.70°, and 77.38° corresponding to (220), (311),

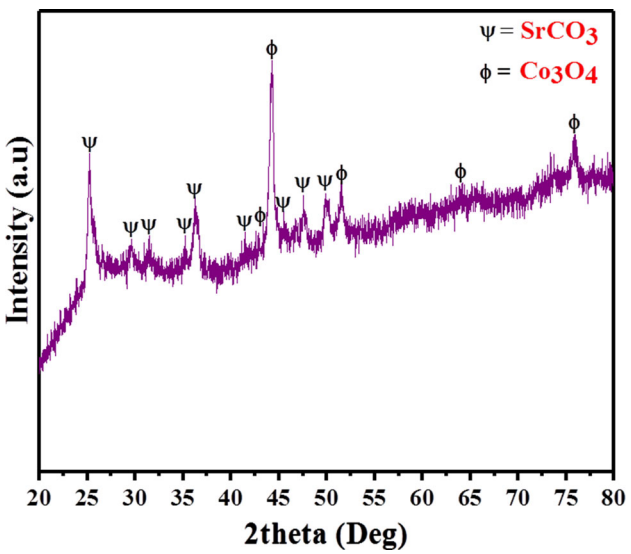

Fig. 1 XRD pattern for the obtained Co_3O_4–$SrCO_3$ heterostructure nanorods-incorporated. CNFs after calcination at 750 °C for 6 h in inert environment

(400), (422), and (533) reflection planes, respectively, of the cubic spinel crystalline structure of Co_3O_4 (JCPDS no.: 42-1467).

The phases of synthesized Co_3O_4–$SrCO_3$ heterostructure nanorods-incorporated CNFs are additionally confirmed by Raman spectroscopy. A typical Raman spectrum presented in Fig. 2 exhibits two set of active bands at 478 and 520 cm^{-1} corresponding to the E_g and F_{2g} symmetry modes of Co_3O_4, respectively (Alvarez et al. 2012). The weak band located at around 608 cm^{-1} is also accounted for F_{2g} mode of Co_3O_4 (Cheng et al. 1998). The two high-intensity Raman modes at 181 (caused by in-plane bending) and 700 cm^{-1} [comes from librational motion of the $(CO_3)^{2-}$] are attributed to the vibration bands of $SrCO_3$ (Divya 2016). In addition, two significant bands were also observed at 1359 and 1595 cm^{-1}, which are assigned to the D- and G-bands of carbon nanofibers, respectively.

FTIR spectra (Fig. 3) of synthesized Co_3O_4–$SrCO_3$ heterostructure nanorods-incorporated CNFs were recorded over the 400–4000 cm^{-1} wavenumbers. Commonly, the free-planar CO_3^{2-} complexes have D_{3h} symmetry and the absorption bands were produced by the vibrations in CO_3^{2-} complex ions at 400–1800 cm^{-1} wavenumbers. The two strong absorption bands (located at around 1463 and 855 cm^{-1}) and one weak absorption band (located at around 1064 cm^{-1}) for $SrCO_3$ are assigned to be out-of-plane and in-plane bending vibrations (Choi and Huh 2009; Davar et al. 2011). In addition, further two absorption bands are located at 580 and 664 cm^{-1}, indicating the presence of typical stretching vibrations of Co–O group in Co_3O_4 (Shahabuddin et al. 2016). Moreover, the absorption peak at around 1670 cm^{-1} corresponds to the O–H group in the water molecule (Xu et al. 2016).

Thermal behavior was measured from room temperature to 750 °C by TGA analysis. As shown from the thermograph (Fig. 4), initial weight loss occurred at below 200 °C, due to the removal of physically adsorbed water. The second major weight loss was observed between 200 and 590 °C, due to simultaneous dehydration of structural water and thermal decomposition of acetate ions, and final weight loss that was observed between 590 and 750 °C can

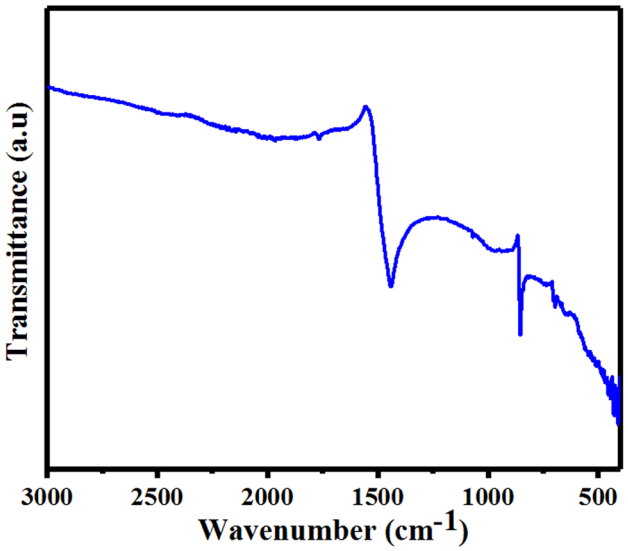

Fig. 3 FTIR pattern for the obtained Co_3O_4–$SrCO_3$ heterostructure nanorods-incorporated. CNFs after calcination at 750 °C for 6 h in inert environment

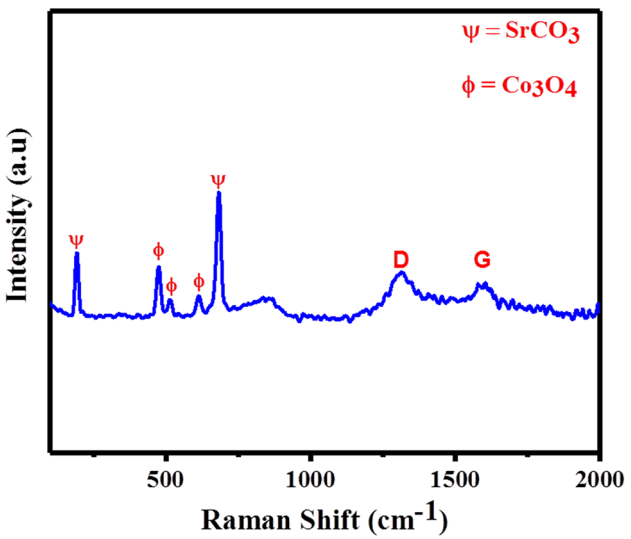

Fig. 2 Raman pattern for the obtained Co_3O_4–$SrCO_3$ heterostructure nanorods-incorporated. CNFs after calcination at 750 °C for 6 h in inert environment

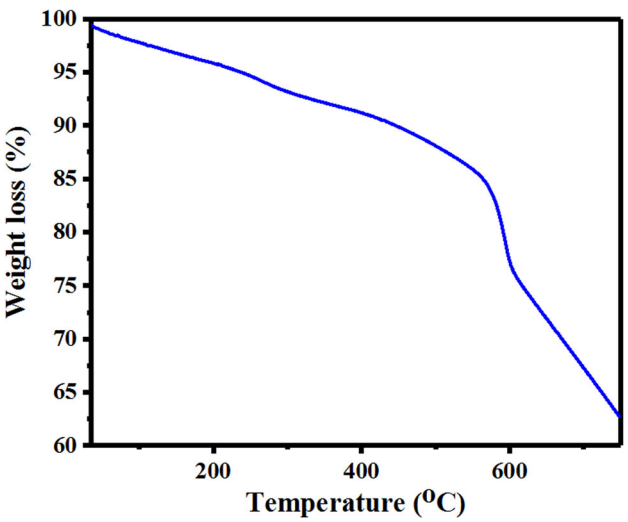

Fig. 4 TGA pattern for the obtained Co_3O_4–$SrCO_3$ heterostructure nanorods-incorporated. CNFs after calcination at 750 °C for 6 h in inert environment

be accounted for the decomposition of polymeric chain and phase transformation.

The morphology of synthesized Co_3O_4–$SrCO_3$ heterostructure nanorods-incorporated CNFs was analyzed by field-emission scanning electron microscope (FESEM). Figure 5a–c shows the FESEM images of the Co_3O_4–$SrCO_3$ heterostructure nanorods-incorporated CNFs at different magnifications. As shown in low-magnification image (Fig. 5a), various dense nanoparticle clusters were observed on the surface of carbon nanofibers. Interestingly, it can be observed that the Co_3O_4–$SrCO_3$ nanoparticles were composed of nanorods with a thickness of $\approx$ 50 nm and average length about 150–200 nm, which were grownup uniformly on the skeleton of carbon nanofibers (Fig. 5b). However, as shown in Fig. 5c, not only nanorods but also nanoballs were observed; it is possible that some nanorods may be vertically aligned and the X-ray beam parallel to those vertically aligned nanorods may result in the observation of nanoballs.

Elemental profile was determined from EDX line scan analysis (Fig. 6) along the selected line. The results confirm that all the carbon, oxygen, strontium, and cobalt signals are dominantly distributed along at the surface of nanofibers.

Considering the preceding information and the fact that nickel-based catalysts have low electrocatalytic activity, it can be electrochemically activated by consecutive cyclic voltammetry sweeping in an alkaline environment for creating NiOOH active layer on the surface, which is mainly responsible for worthy electrochemical activity. According to the following equation, NiOOH ionic layer is responsible for electrooxidation process in direct urea fuel cells (Wang et al. 2014).

$$2CO(NH_2)_2 + 6NiOOH + H_2O \rightarrow 6Ni(OH)_2 + N_2 + CO_2$$

Therefore, it is rational to carry out multiple cyclic voltammetry sweeping to investigate the electrochemical activity of the non-nickel-based electrocatalyst. Figure 7 shows the cyclic voltammogram (CV) of Co_3O_4–$SrCO_3$ heterostructure nanorods-incorporated CNFs electrode in the potential range from -200 to 1000 mV/s (vs. Ag/AgCl) at a scan rate of 50 mV/s in 1.0 M KOH. As shown, current density gradually increases with the number of potential sweeps at low voltage (0.4 V), due to the introduction of OH^- ions into the skeleton of catalyst; this suggests that the adsorption–desorption processes are not reversible. Interestingly, no oxidation/reduction peaks are observed, proposing that the performance of catalyst is independent

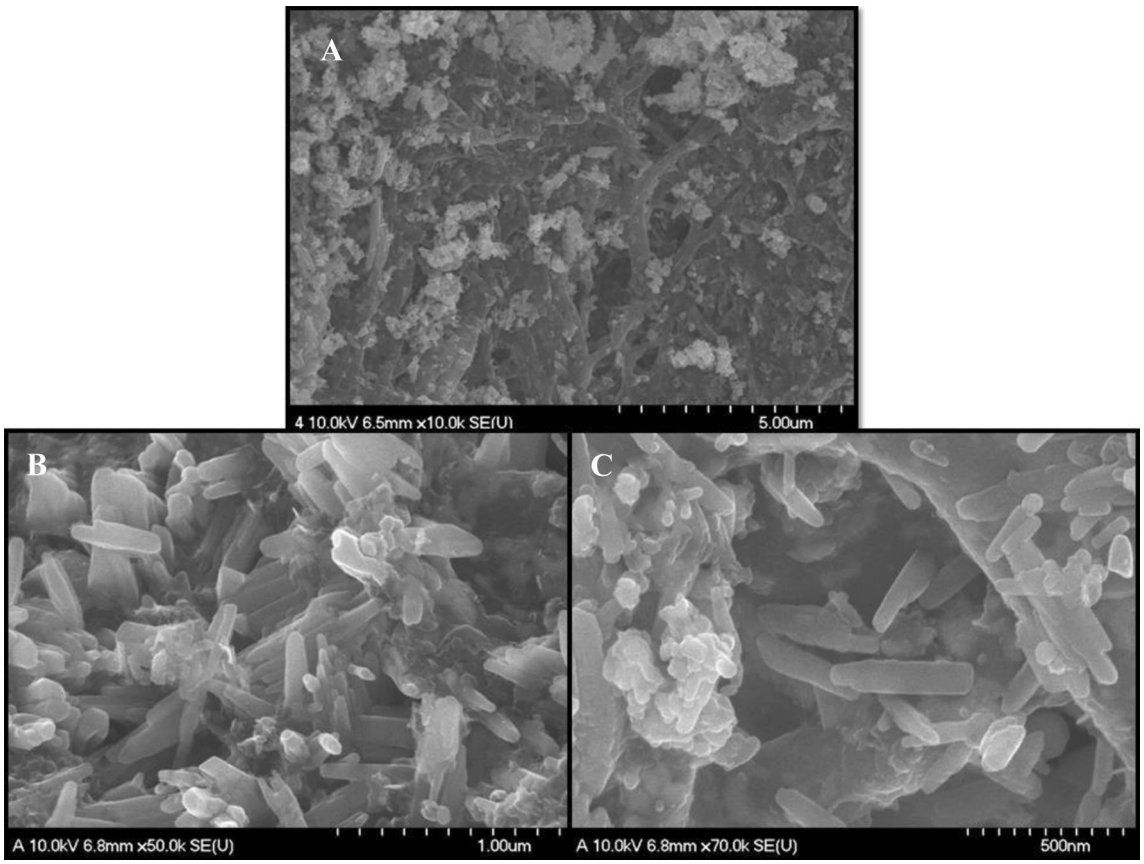

Fig. 5 **a–c** FESEM image of Co_3O_4–$SrCO_3$ heterostructure nanorods-incorporated CNFs after calcination at 750 °C for 6 h in inert environment

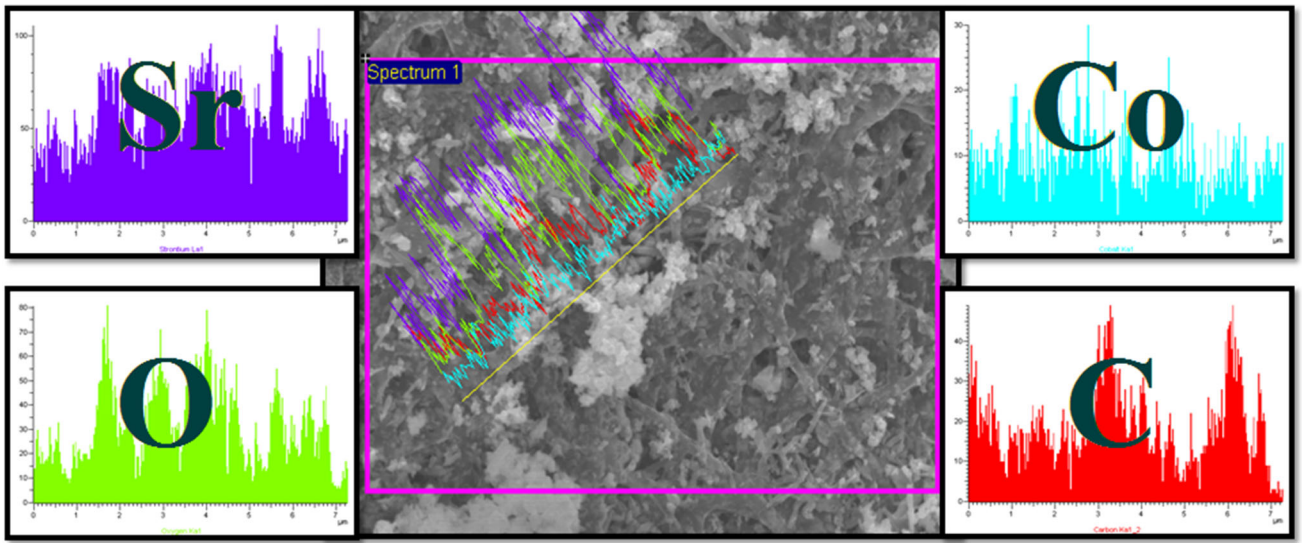

Fig. 6 Line EDX for the obtained Co_3O_4–$SrCO_3$ heterostructure nanorods-incorporated CNFs after calcination at 750 °C for 6 h in inert environment

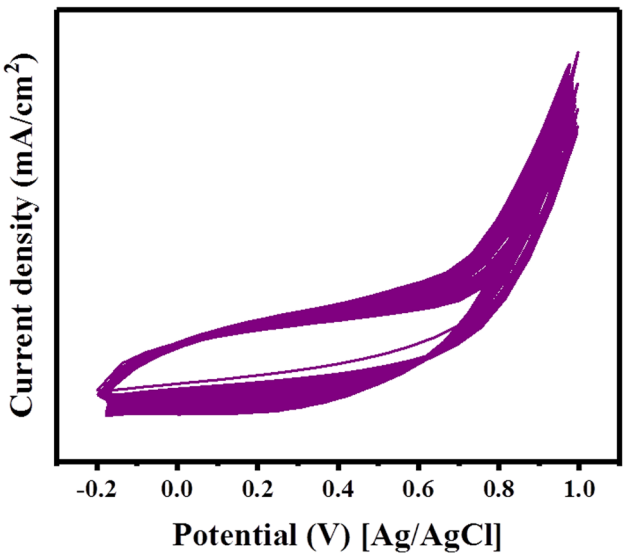

Fig. 7 Cyclic voltammograms for the obtained Co_3O_4–$SrCO_3$ heterostructure nanorods-incorporated CNFs after calcination at 750 °C for 6 h in inert environment at scan rate of 50 mV/s at room temperature

of the formation of active ionic layer; this revealed a good catalytic activity of Co_3O_4–$SrCO_3$ heterostructure nanorods-incorporated CNFs electrode.

Figure 8 displays the cyclic voltammograms (CVs) of Co_3O_4–$SrCO_3$ heterostructure nanorods-incorporated CNFs electrodes in a solution of urea ranging from 0.1 to 3.0 +1.0 M KOH. As shown, polarization was started between −2.0 and 1.0 V under a sweep rate of 10 mV/s vs. Ag/AgCl. As revealed in high magnification voltammogram (Fig. 8b), the presence of urea in the alkaline solution has strong influence on anodic current density. However, the observed low-current density at high urea concentration (1.0, 2.0, and 3.0) is understandable due to kinetics limitations of electrode material. Interestingly, no significant difference was observed among the maximum current density obtained from 0.5 and 0.33 M urea concentration that may be due to a diffusion controlled process. Regardless of high-current density (29.5@0.33 M urea), the onset potential at which the urea electrooxidation actually starts is considered as a key factor to influence the direct urea fuel cell performance. As shown in Fig. 8c, the minimum onset potential observed was 0.5 V vs. Ag/AgCl, which is very low compared to non-nickel-based catalysts. This could be caused by the exposed active sites of the Co^{3+} ions, which would act as donor-acceptor reduction sites on the surface of Co_3O_4–$SrCO_3$ nanostructures. In addition, Co^{3+} ions can produce surface electronic states by Jahn–Teller effect in alkaline media, which can be predicted as the active sites for the alkaline electrocatalytic reactions (Unwin and Compton 1989). Moreover, these results could not only be accredited to the unique architecture of electrode which would supply more active sites for urea electrooxidation, but incorporation of $SrCO_3$ in cobalt oxide increases the structural defects of cobalt oxide which lead to providing convenient electroactive pathway for rapid ionic transformation on the surface of electrode during urea electrooxidation. Probably, the conductive network of carbon with strongly attached nano-metallic counterparts not only adsorbs greater number of urea

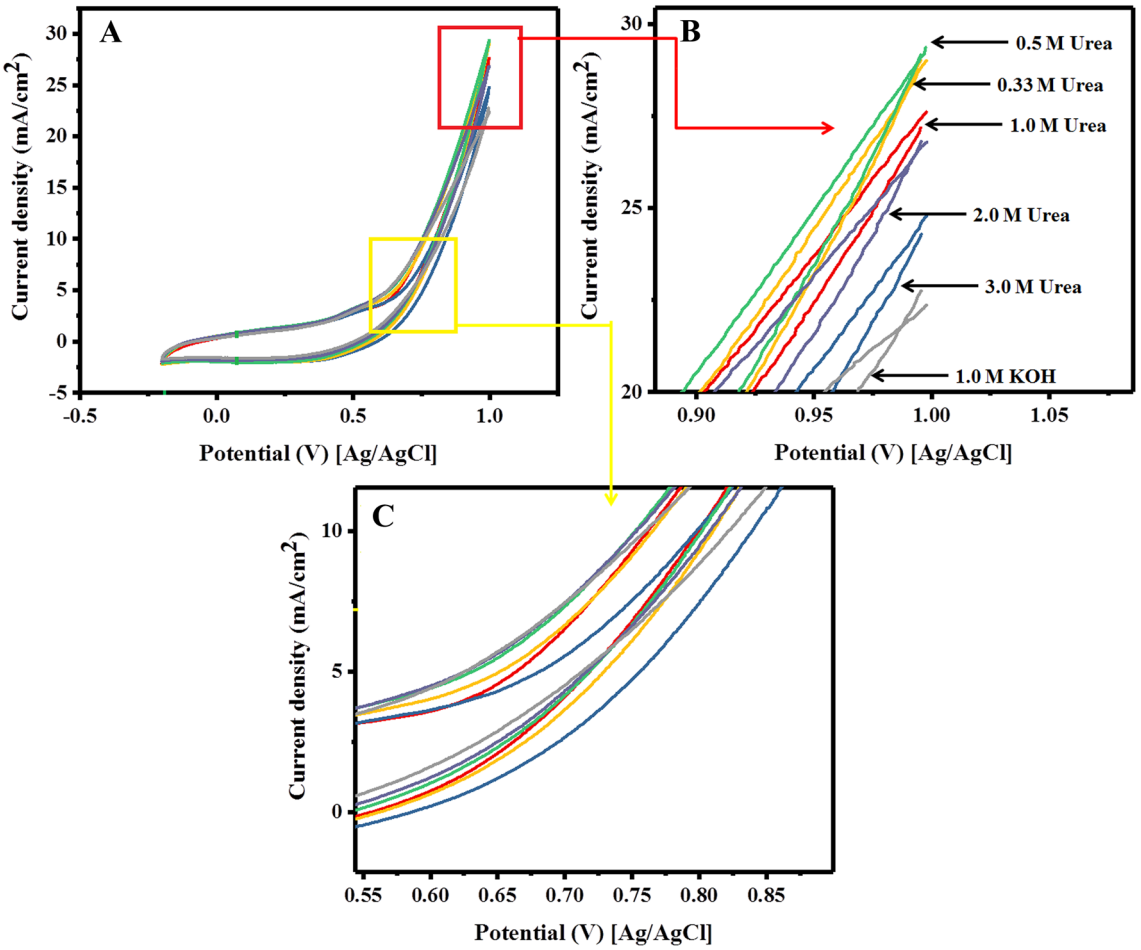

Fig. 8 **a** Typical Cyclic voltammograms for the obtained Co_3O_4–$SrCO_3$ heterostructure nanorods-incorporated CNFs in different concentrations of urea (+1 M KOH), **b** high magnification to show the influence of urea concentration on current density, and **c** high magnification to show the onset potential at scan rate of 50 mV/s at room temperature

molecules but is capable of electrooxidation of urea at low-onset potential with high-current density.

Conclusions

In conclusion, we have successfully synthesized nickel-free electrocatalyst based on Co_3O_4–$SrCO_3$ heterostructure nanorods-incorporated CNFs, by a simple electrospinning technique followed by a thermal treatment in inert environment at 750 °C. The resultant Co_3O_4–$SrCO_3$ heterostructure nanorods-incorporated CNFs exhibit high-current density at low-fuel concentration. Remarkably, because of good conductive network of carbon nanofibers with high dispersion of metallic counterpart on the surface of carbon nanofibers support, the nickel-free electrode was capable of lowering the onset potential toward urea electrooxidation, representing hopeful applications in direct urea fuel cells anodes.

Acknowledgements This Publication was made possible by NPRP grant # [8-1344-1-246] from the Qatar National Research Fund (a member of Qatar Foundation). The findings achieved herein are solely the responsibility of authors.

References

Alvarez A et al (2012) Sub-ambient CO oxidation over mesoporous Co_3 O_4: effect of morphology on its reduction behavior and catalytic performance. Appl Catal A 431:9–17

Boggs BK, King RL, Botte GG (2009) Urea electrolysis: direct hydrogen production from urine. Chem Commun 32:4859–4861

Chen J-D et al (2015) Easy-to-prepare electrochemical platform composed of ionic liquid-Ni(II)-graphite composites: laboratory

study on electrochemical oxidation of urea, alcohols, and glucose. Electrochim Acta 182:113–121
Cheng C-S et al (1998) Electrical conductivity of Co_3 O_4 films prepared by chemical vapour deposition. Mater Chem Phys 53(3):225–230
Choi E-J, Huh Y-D (2009) Preparation of elongated hexagonal pyramids and hexagonal prisms of SrCO3 using hydrothermal reactions. Bull Korean Chem Soc 30(9):2132–2134
Davar F, Salavati-Niasari M, Baskoutas S (2011) Temperature controlled synthesis of SrCO3 nanorods via a facile solid-state decomposition rout starting from a novel inorganic precursor. Appl Surf Sci 257(9):3872–3877
Divya A et al (2016) Experimental and theoretical spectroscopic studies of branchlet-like $SrCO_3$ superarchitecture. In: AIP conference proceedings. AIP
Ghouri ZK et al (2015a) Co/CeO_2-decorated carbon nanofibers as effective non-precious electro-catalyst for fuel cells application in alkaline medium. Cerami Int 41(2):2271–2278
Ghouri ZK, Barakat NA, Kim HY (2015) Influence of copper content on the electrocatalytic activity toward methanol oxidation of CoχCuy alloy nanoparticles-decorated CNFs. Sci Rep **5**
Ghouri ZK et al (2016) Nano-engineered ZnO/CeO_2 dots@ CNFs for fuel cell application. Arab J Chem 9(2):219–228
Guo F et al (2015) Preparation of nickel nanowire arrays electrode for urea electro-oxidation in alkaline medium. J Power Sources 278:562–568
Hu L, Peng Q, Li Y (2008) Selective synthesis of Co_3O_4 nanocrystal with different shape and crystal plane effect on catalytic property for methane combustion. J Am Chem Soc 130(48):16136–16137
Jiao F, Frei H (2009) Nanostructured cobalt oxide clusters in mesoporous silica as efficient oxygen-evolving catalysts. Angew Chem Int Ed 48(10):1841–1844
Kim JY et al (2014) A hollow assembly and its three-dimensional network formation of single-crystalline Co_3O_4 nanoparticles for ultrasensitive formaldehyde gas sensors. J Phys Chem C 118(45):25994–26002
King RL, Botte GG (2011) Investigation of multi-metal catalysts for stable hydrogen production via urea electrolysis. J Power Sources 196(22):9579–9584
Kojima S, Bohner A, Von Wirén N (2006) Molecular mechanisms of urea transport in plants. J Membr Biol 212(2):83–91
Lan R, Tao S (2011) Preparation of nano-sized nickel as anode catalyst for direct urea and urine fuel cells. J Power Sources 196(11):5021–5026
Lan R, Tao S, Irvine JT (2010) A direct urea fuel cell–power from fertiliser and waste. Energy Environ Sci 3(4):438–441
Li W-Y, Xu L-N, Chen J (2005) Co_3O_4 nanomaterials in lithium-ion batteries and gas sensors. Adv Func Mater 15(5):851–857
Li Y, Tan B, Wu Y (2008) Mesoporous Co_3O_4 nanowire arrays for lithium ion batteries with high capacity and rate capability. Nano Lett 8(1):265–270
Radenahmad N et al (2016) Proton-conducting electrolytes for direct methanol and direct urea fuel cells—a state-of-the-art review. Renew Sustain Energy Rev 57:1347–1358
Shahabuddin S et al (2016) Synthesis and characterization of Co_3O_4 nanocube-doped polyaniline nanocomposites with enhanced methyl orange adsorption from aqueous solution. RSC Adva 6(49):43388–43400
Shahid MM et al (2014) Enhanced electrocatalytic performance of cobalt oxide nanocubes incorporating reduced graphene oxide as a modified platinum electrode for methanol oxidation. RSC Adv 4(107):62793–62801
Unwin PR, Compton RG (1989) The use of channel electrodes in the investigation of interfacial reaction mechanisms. Compr Chem Kinet 29:173–296
Wang D et al (2013) Electrochemically reduced graphene oxide–nickel nanocomposites for urea electrolysis. Electrochim Acta 89:732–736
Wang L et al (2014) Ni–WC/C nanocluster catalysts for urea electrooxidation. J Power Sources 264:282–289
Xu W et al (2014) Nickel-cobalt bimetallic anode catalysts for direct urea fuel cell. Sci Rep 4:5863
Xu W, Wu Z, Tao S (2016a) Urea-based fuel cells and electrocatalysts for urea oxidation. Energy Technol 4(11):1329–1337
Xu B et al (2016b) Cobalt modified red mud catalytic ozonation for the degradation of bezafibrate in water: catalyst surface properties characterization and reaction mechanism. Chem Eng J 284:942–952

Publisher's Note